

Neutral-pion photoproduction and proton Compton scattering at large angles

M. A. Shupe,* R. H. Milburn, D. J. Quinn,[†] J. P. Rutherford,[‡] and A. R. Stottlemyer[§]
Tufts University, Medford, Massachusetts 02155

S. S. Hertzbach, R. R. Kofler, F. D. Lomanno, and M. S. Z. Rabin
University of Massachusetts, Amherst, Massachusetts 01002

M. Deutsch and M. M. White
Massachusetts Institute of Technology, Cambridge, Massachusetts 02139

R. S. Galik^{||} and R. H. Siemann
Cornell University, Ithaca, New York 14853

(Received 6 March 1978; revised manuscript received 17 November 1978)

The differential cross sections for $\gamma p \rightarrow \gamma p$ and $\gamma p \rightarrow \pi^0 p$ have been measured for incident photon energies in the range of 2 to 6 GeV and for $|t|$ ranging from 0.7 to 4.3 GeV². This corresponds to a center-of-mass angle range of 45° to 128°. The energy dependence of the data is compared to that predicted by several parton models.

I. INTRODUCTION

Previous experiments¹ on proton Compton scattering concentrated on the small- $|t|$ region allowing comparisons of the forward differential cross section with optical-theorem² and dispersion-relation³ predictions and with the vector-dominance model. The exponential slope in t and nearly energy-independent forward cross section seen in these experiments are characteristic of purely diffractive scattering. Measurements of the polarized-photon asymmetry⁴ and the recoil-proton polarization⁵ have supported this interpretation of forward Compton scattering as a diffractive process. Various models^{6,7} which predict that this behavior would not extend much beyond the range of existing data have not been tested because of difficulties in measuring the very small cross sections at larger $|t|$.

Neutral-pion photoproduction has also been studied extensively at small $|t|$.⁸ Most of this work was motivated by interest in the Regge exchanges which dominate the forward cross section. Similar interests in baryon exchange led to some cross-section measurements in the backward direction,⁹ the region of small $|\mu|$.

Dimensional-counting arguments,⁷ which make predictions for many processes, suggest that mechanisms other than Regge exchanges will dominate π^0 photoproduction in the central region between small $|t|$ and $|\mu|$. Several experimental groups have made measurements in this region,^{10,11} but the conclusions are not completely clear because of disagreements between these data.

This experiment was designed to explore the region around 90° in the center of mass primarily

to make the first measurements of large-angle Compton scattering, but also to extend, somewhat, the energy range for π^0 photoproduction. Since both processes are measured in the same experiment, the ratio of cross sections can be accurately determined. The differential cross sections from a hydrogen target were measured for angular sweeps at 3 and 4 GeV and energy sweeps at $t = -2.45$ GeV² and at center-of-mass angles of 60°, 90°, and 105°. Results of the experiment have been published elsewhere.¹² In this paper we discuss the experiment in greater detail and present comparisons with appropriate models.

II. EXPERIMENT

The experiment was performed at the Wilson 12-GeV Electron Synchrotron at Cornell University. The incident photons were generated by an extracted electron beam focused to a spot approximately 3 mm in diameter on a 0.10-radiation-length aluminum target. The electrons in the resulting beam were magnetically diverted into a water-cooled dump. The bremsstrahlung photon beam passed through a collimator, sweeping magnet, scraper, and another sweeping magnet before entering the hydrogen target which was 11.5 m downstream of the radiator. At this point the beam was about 1.3 cm in diameter at the lowest energy. The hydrogen target cup was a cylinder 6.35 cm long by 5.08 cm in diameter oriented with its axis coincident with the beam direction. The end windows were each 18- μ m-thick stainless steel.

The noninteracting photons proceeded through a long helium bag to a secondary-emission monitor

(SEM) well downstream of (and shielded from) the detection apparatus. This SEM was placed behind 5 radiation lengths of lead, and it measured the number of equivalent quanta in the beam. At each electron beam energy, the calibration of the SEM was compared with that of a laboratory standard secondary-emission quantameter. The SEM calibration constant was found to vary by 6% over the range of energies used in this experiment; this variation was consistent with previous measurements. A thick target bremsstrahlung calculation¹³ gave the number of incident photons in an energy band from the number of equivalent quanta. Uncertainties in the calibration procedure, the standard quantameter calibration, and the bremsstrahlung calculation lead to net uncertainties of $\pm 3\%$ in the incident flux at most half of which is energy dependent.

Reactions of interest were separated by their kinematics. The technique required measurement of the momentum and angles of the recoil proton and the angles of one photon, either Compton scattered or from the decay of a π^0 (see Fig. 1). The energy of the photon was also measured, but this constraint was not used in the determination of the kinematics. Cuts on this energy were used to eliminate some background effects particularly for π^0 events.

The proton emerging from the target passed through a small permanent dipole magnet (of approximately 0.02 T m) intended to sweep away low-energy particles, through five multiwire pro-

portional chamber (MWPC) planes and then into the Cornell Large Aperture Spectrometer (CLASP).¹⁴ CLASP consisted of a vertical-bend dipole magnet, eight MWPC planes interleaved with four trigger hodoscope counter planes, a threshold gas Čerenkov counter set to count pions, and finally, a lead-Lucite shower counter to discriminate against positrons. The magnet aperture was 20.3 cm wide by 38.1 cm high, and the pole pieces were 121.9 cm long. The maximum field was about 1.85 T. The momentum acceptance of the spectrometer, which was far wider than necessary for the two-body reactions studied here, was approximately $\Delta p/p = +30\%$ (-80%), and the solid angle at the nominal momentum was about 4 msr.

One MWPC in front of the magnet had sense wires running vertically, while the sense wires of the other four MWPC's were tilted alternately $\pm 7^\circ$ to the horizontal to minimize dead-time losses. This configuration allowed excellent measurements of the vertical angle of the proton [1.0 mrad rms] and the height of the interaction in the target [0.3 cm (rms)] and, hence, coplanarity of the detected particles with the beam. Chambers behind the magnet were used in conjunction with the one vertical MWPC in the front to measure the horizontal angle and target position. Typical horizontal-angle resolution was 1.5 mrad (rms). The momentum was calculated from the vertical slopes of the trajectory in front of and behind the magnet using an effective length approximation for the magnetic field integral. The momentum resolution was approximately 1% (rms) and was dominated by multiple scattering of the proton in the air and MWPC's at low momentum and by field inhomogeneities at high momentum. The momentum and horizontal-angle resolutions gave a resolution in incident energy of 0.08 GeV (rms) and in t of approximately 1% (rms). All MWPC's had wire spacings of 1.27 mm, giving a total of 4656 wires in the system.

The direction of the outgoing photon was determined using a 72-block lead-glass detector consisting of two side-by-side arrays of 36 blocks each, positioned transverse to the average photon direction (see Fig. 1 inset).¹⁴ The 36 blocks of Schott SF2 lead glass, each 6.35 cm by 6.35 cm by 58.4 cm, were arrayed four stacks deep (a total of 9 radiation lengths) and nine blocks high. Successive stacks were vertically offset by $\frac{1}{3}$ block height to improve position resolution by analysis of the energy sharing between blocks. An array of scintillation counters (3.8 cm wide) inserted after the second layer of blocks measured the horizontal position. Resulting position resolutions were 1.3 cm [full width at half maximum (FWHM)] in the vertical¹⁵ and 3.8 cm (FWHM) in

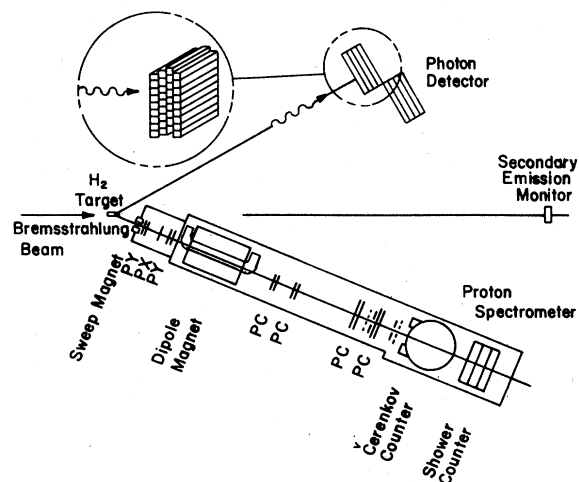


FIG. 1. Schematic floor plan of the apparatus. PY designates a pair of MWPC's with wires at $\pm 7^\circ$ to the horizontal, PX an MWPC with vertical wires, PC a pair of MWPC's with wires horizontal and vertical, and TH a scintillation counter trigger hodoscope. A perspective view of one of the two lead-glass arrays is depicted in the inset.

the horizontal. This gave photon angle resolutions dependent on the distance of the lead-glass detector from the hydrogen target. This distance was varied from data point to data point (4.0 m to 12.8 m) and gave a reasonable match to the vertical angle resolution on the proton arm. The energy resolution was on the order of 30% (rms) at all energies.

The event trigger required a time coincidence between an energetic shower in the lead-glass and the firing of any three out of four counter planes in the spectrometer. At each data point the lead-glass trigger threshold was set to one-half the minimum energy of a photon from π^0 decay. In determining this threshold we considered only π^0 's which would pass our event reconstruction criterion that the π^0 be directed towards the lead-glass detector. By requiring only three out of four spectrometer counter planes, we were able to measure the trigger efficiency of the proton arm.

The incident beam flux was typically 1.2×10^{10} equivalent quanta per second, close to the maximum available from the synchrotron with our radiator. At this intensity the Compton scattering rate ranged from 50 to 0.1 events per hour; the rate of π^0 events was approximately 50 times the Compton scattering rate. At each data point the beam flux was limited by either singles rates in the proportional chambers closest to the target (2 MHz per wire was the maximum rate allowed in these chambers) or by accidental coincidences. Because of the loose trigger requirements and the high beam intensity, between 40% and 70% of the trigger rate was due to accidentals.

In approximately one-half of the triggers, trajectories from the target could be spatially reconstructed in the spectrometer. The remainder were largely random coincidences, as indicated by measurements of the time-of-flight difference between the photon and the proton. In general, when a spectrometer trajectory failed reconstruction, there also was no corresponding analyzable shower in the lead-glass. Therefore, most of the bad triggers were eliminated by any one of three criteria: an incorrect time-of-flight, no trajectory in the proton spectrometer, or no analyzable shower in the lead glass. Only those triggers with a single high-energy shower (the two photon acceptance was almost zero) and a reconstructed track passed our cuts. We discuss below the corrections necessary because of these selection criteria. The CLASP shower and gas Čerenkov counters showed that this sample of data had negligible pion and positron contamination.

For these events, the reaction plane was defined by the incident photon direction (well determined

in the vertical plane by the radiator spot and the target position) and the recoil proton trajectory. The photon production angle and momentum were predicted from the proton four-vector assuming $\gamma p \rightarrow \gamma p$ kinematics. The angular differences between the observed photon and predicted photon directions in the reaction plane, $\Delta\theta$, and perpendicular to the reaction plane (coplanarity), $\Delta\phi$, were then found. Typical resolutions in $\Delta\theta$ and $\Delta\phi$ were 20 mrad and 5 mrad (FWHM).

In Fig. 2 we present coplanarity distributions with and without a $\Delta\theta$ cut. At this data point (which has a large Compton-scattering signal) the enhancement at $\Delta\phi = 0$ is evident even without the production-angle cut. Imposing this cut reduces the π^0 and background signals without significantly depleting the Compton scattering signal.

The $\Delta\phi$ and $\Delta\theta$ distributions were used to determine the relative contributions of different

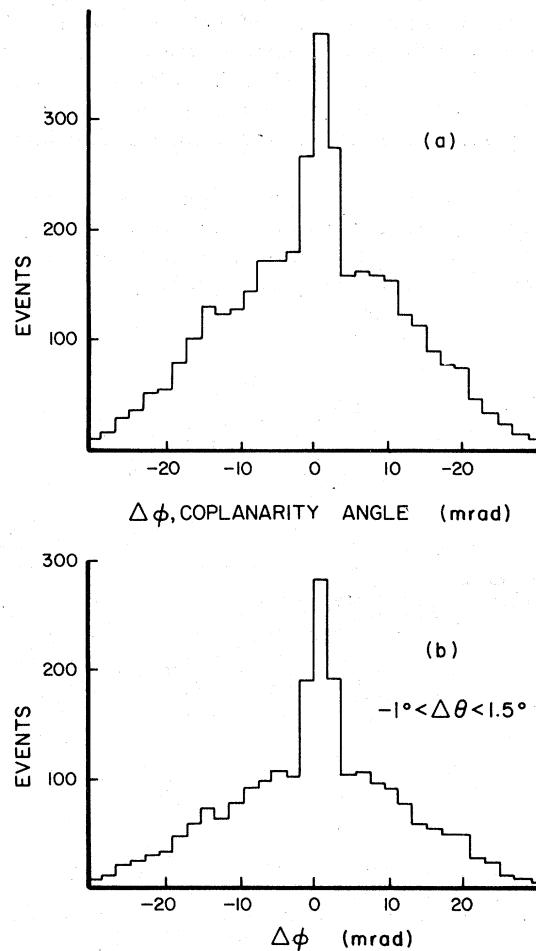


FIG. 2. Coplanarity distributions at 3 GeV and $t = 0.71$ GeV². (a) without and (b) with a cut on the $\Delta\theta$.

processes to our data. A Monte Carlo calculation was used to calculate the distributions expected for single- π^0 photoproduction and proton Compton scattering. The coplanarity data with different $\Delta\theta$ cuts were then fit to a combination of these distributions and a smooth empirical background. It was found that over a large range of $\Delta\theta$ cuts, the Compton scattering cross section and its error did not change significantly. The final $\Delta\theta$ cut was chosen in this range. The data with $\Delta\theta$ outside of the final cuts were useful for separating π^0 photoproduction from background. At some data points as much as 20% of the events were from background processes.

The philosophy of the fitting procedure can now be made more clear. The coplanarity distribution was used almost exclusively to determine the Compton scattering signal. This can be done with good accuracy only if the shape of the distribution of the rest of the data is well known. It is the $\Delta\theta$ distribution which assures us that single- π^0 photoproduction is the dominant process. Since the π^0 decay kinematics and the detector are well understood, the shape of the coplanarity distribution is determined.

In Fig. 3 we present more typical coplanarity and $\Delta\theta$ distributions with curves drawn to show the contributions of the background and π^0 photoproduction. The ratio of events from Compton scattering to those from π^0 photoproduction in the coplanarity peak was in the range of 1:1 to 1:4 for all the data. The separation of Compton scatters from the more copious π^0 photoproduction is cru-

cially dependent on the coplanarity resolution, about 5 mrad (FWHM). For data points where the statistics were good, the resolution could be treated as a free parameter, and the resultant resolution was in good agreement with that calculated by the Monte Carlo. For low-statistics points we constrained the resolution to be that given by the Monte Carlo program.

We performed a Monte Carlo calculation of the acceptance parameters with an accuracy better than the statistical errors of the Compton scattering data. A small empty-target correction (1%) was made only to the neutral-pion photoproduction cross section. Fermi motion of the nucleons in the stainless-steel endcaps on the hydrogen target spreads the Compton-scattering coplanarity peak by an amount comparable to the width of the π^0 distribution. Large corrections were made to both π^0 and Compton scattering cross sections for proton and photon identification inefficiencies discussed below.

The proton-spectrometer inefficiency was calculated in two steps. The combination of low rate and redundant detectors behind the magnet allowed the rear detector inefficiency to be found by calculating trigger counter (~4%) and MWPC inefficiencies (~3%). The trigger-counter inefficiency includes nuclear absorption effects. In each view hits in at least three of the four MWPC's were needed to form a track, and we required a single track in each view. All single good tracks in the back projecting through the magnet to the front detector were assumed to have traversed the entire spectrometer and were used to find the inefficiency of the front MWPC's in their high-rate environment. Hits were required within ± 1.27 cm of the projected track in four out of five front chambers. Typically 27% of the tracks failed this cut. Those passing this cut were required to have a good track in the front chambers; typically 6% failed this requirement. The inefficiency of these chambers was the largest contribution to the proton inefficiency. The net inefficiency was typically 40% with an estimated uncertainty of 10%. Of this, 9% is an overall uncertainty, leaving 4% estimated point-to-point systematic uncertainty. The various inefficiencies were found to be correlated with each other. At each data point this correlation was studied by using data samples with different cuts. The result was bracketed by choosing cuts which clearly either overestimated or underestimated the net inefficiency. The width of the bracketed region was taken as the uncertainty. The systematic uncertainties in the proton detection efficiency are the same for Compton scattering and π^0 photoproduction, and they cancel when taking the ratio of these cross sections.

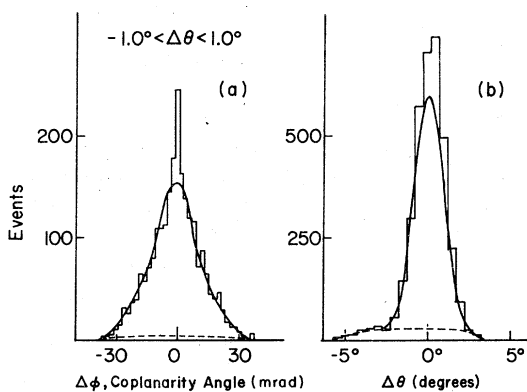


FIG. 3. Angular-difference distribution at 6 GeV and $t = -2.45 \text{ GeV}^2$. (a) Coplanarity-angle distribution. The solid line is a fit assuming neutral-pion photoproduction, the dashed line is the estimated background from other processes, and the peak at $\Delta\phi = 0$ is due to proton Compton scattering. (b) Angular-difference distribution in the reaction plane. The curves have the same interpretation as in (a). The excess at $\Delta\theta = 0^\circ$ is due to Compton scattering.

TABLE I. Typical corrections and systematic uncertainties. The larger corrections and uncertainties are discussed in the text. Under uncertainty, the first column contains errors which affect the overall normalization only; the second includes errors which can fluctuate from data point to data point; and the third exhibits the systematic errors in the Compton scattering to π^0 photoproduction cross-section ratio.

| | Typical corrections | Overall | Uncertainty Point-to-point | Ratio |
|---|------------------------|-------------|-------------------------------|------------|
| Proton-arm inefficiency | | | | |
| Trigger counter | 4% | $\pm 1\%$ | $\pm 1\%$ | $\pm 0\%$ |
| Rear MWPC | 3% | $\pm 1\%$ | $\pm 1\%$ | $\pm 0\%$ |
| Front MWPC | 33% | $\pm 9\%$ | $\pm 4\%$ | $\pm 0\%$ |
| Photon-arm inefficiency | 30% | $\pm 9\%$ | $\pm 5\%$ | $\pm 8\%$ |
| Beam flux | 0% | $\pm 3\%$ | $\pm 1.5\%$ | $\pm 0\%$ |
| Target length and density | 0% | $\pm 1\%$ | $\pm 1\%$ | $\pm 0\%$ |
| Computer dead times | 8% | $\pm 0\%$ | $\pm 0\%$ | $\pm 0\%$ |
| Trigger dead time | 0.5% | $\pm 0.5\%$ | $\pm 0.5\%$ | $\pm 0\%$ |
| Absolution calibration of spectrometer | 0% | $\pm 7\%$ | $\pm 2\%$ | $\pm 4\%$ |
| Data lost | 0.2% | $\pm 0\%$ | $\pm 0\%$ | $\pm 0\%$ |
| Fitting hypotheses | 0% | $\pm 5\%$ | $\pm 4\%$ | $\pm 5\%$ |
| Net uncertainty | | $\pm 20\%$ | $\pm 8\%$ | $\pm 10\%$ |

The lead-glass gave nearly 100% positive identification of a shower, but shower fluctuations and low energy, time-random backgrounds often confused the pattern recognition algorithm. This algorithm relied on a series of stringent tests in selecting a sample of showers which developed clearly enough to guarantee good position measurements. To learn the efficiency of this pattern recognition, a shower identification program was written which ensured the presence of a high-energy shower without requiring a good position measurement. Monte Carlo generated showers were used to check these programs, and experimental data taken in a positron test beam were in turn used to check this Monte Carlo. The resultant inefficiency for photon identification was found to be energy dependent, ranging from 40% at 1 GeV to 15% at greater than 3 GeV. The bulk of this energy dependence at a given data point came from the inefficiency of the embedded hodoscope counters, which was near 0% for showers above 3 GeV. The rest came from the sea of very-low-energy, time-random showers which made identification of valid lower-energy showers more difficult. This low-energy background changed from data point to data point; the photon-arm inefficiency was roughly 30% at all data points. The estimated net uncertainty is 10% of which 5% is a point-to-point systematic uncertainty and 9% is an overall uncertainty. These errors combine estimates using different cuts on the data (as done for the proton arm) with a larger uncertainty to account for the procedure. The systematic uncertainty does not cancel entirely in the ratio of Compton scattering to π^0 photoproduction cross

sections because the photon energy depends on the process. It is estimated that the residual systematic uncertainty in the ratio is 8%.

These, as well as several smaller corrections to the data are summarized in Table I along with a few other contributions to the normalization uncertainty. Because the cross-section dependence on incident energy and t is so steep, the small uncertainty in the CLASP magnetic-field-integral calibration introduces a non-negligible cross-section uncertainty. Most of this uncertainty is in the overall normalization. Of the remaining uncertainties, the only one of importance comes from the small residual uncertainty in the shape of the π^0 distribution used in coplanarity fits. This is caused by approximations made in the Monte Carlo program to the properties of the apparatus.

The net overall systematic uncertainty in the data is 20%, and the net point-to-point systematic uncertainty is 8%. Many of these systematic problems cancel in the cross-section ratio leaving a systematic error of 10%. Correlations in these uncertainties have been estimated and are included in the net quoted values. In general, the systematic errors were larger than the statistical errors for the π^0 data, but smaller than those of the Compton-scattering data.

III. RESULTS AND DISCUSSION

The results are shown in Fig 4 and are given in Table II.

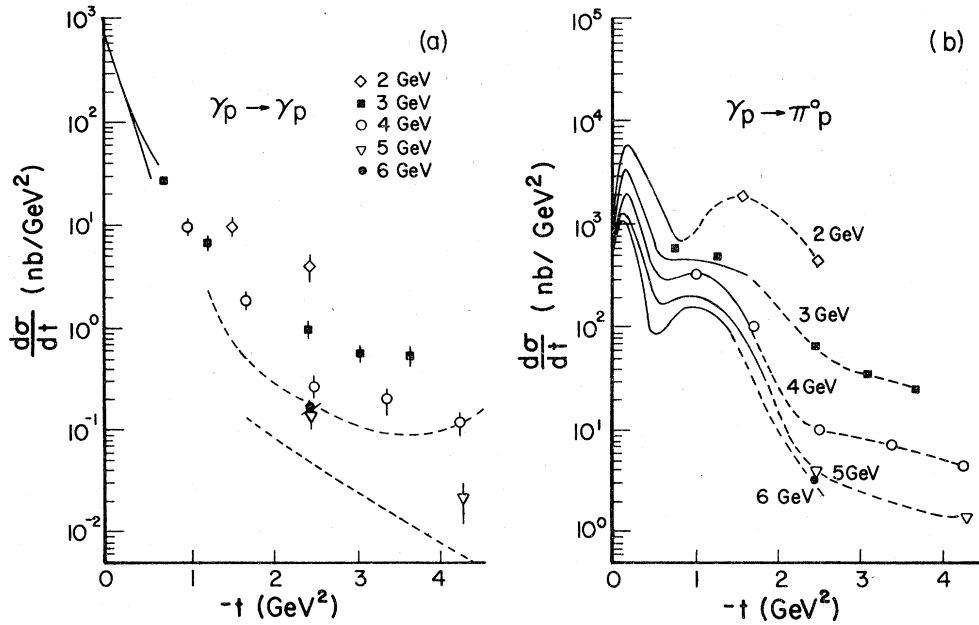


FIG. 4. Data from this experiment. The indicated energies are incident photon laboratory energies. (a) Proton Compton-scattering differential cross sections. The solid lines summarize data from previous experiments, and the split represents either energy dependence or a disagreement between experiments. The dashed line and dotted line are VDM predictions at 4 GeV and 6 GeV, respectively. The error bars include statistical and systematic errors which vary from point to point. (b) $d\sigma/dt$ versus t for π^0 photoproduction. The solid lines summarize earlier data at small $|t|$. The dashed lines are intended only to guide the eye. In general, error bars resulting from statistical errors and systematic errors which vary from point to point are smaller than the size of the data points. Overall systematic errors are not included.

TABLE II. The results of this experiment. The cross-section errors include statistical and point-to-point systematic errors. The errors on the ratio R are only statistical and are larger than the systematic errors. k is the central incident photon energy. Δk is the spread of photon energies about the central value. t is the central four-momentum transfer. Δt is the rms spread of t . θ^* is the photon scattering angle for $\gamma p \rightarrow \gamma p$ in the γ center of mass. R is the ratio of Compton scattering to π^0 photoproduction cross sections.

| k (GeV) | Δk | t (GeV ²) | Δt | θ^* | $\frac{d\sigma}{dt}(\gamma p \rightarrow \gamma p)$ (nb/GeV ²) | $\frac{d\sigma}{dt}(\gamma p \rightarrow \pi^0 p)$ | R |
|--------------|------------|----------------------------|------------|------------|---|--|-----------------|
| 2.0 | 0.23 | -1.52 | 0.19 | 90° | 9.5 ± 1.6 | 1820 ± 115 | 0.0052 ± 0.0012 |
| 2.0 | 0.24 | -2.45 | 0.34 | 128° | 4.0 ± 1.3 | 437 ± 47 | 0.0091 ± 0.0034 |
| 3.0 | 0.38 | -0.71 | 0.08 | 45° | 27.5 ± 2.2 | 560 ± 36 | 0.049 ± 0.005 |
| 3.0 | 0.37 | -1.22 | 0.13 | 60° | 6.9 ± 1.1 | 468 ± 31 | 0.015 ± 0.003 |
| 3.0 | 0.35 | -2.43 | 0.26 | 90° | 0.97 ± 0.19 | 62.8 ± 5.1 | 0.015 ± 0.004 |
| 3.0 | 0.34 | -3.06 | 0.35 | 105° | 0.55 ± 0.11 | 35.4 ± 2.7 | 0.016 ± 0.004 |
| 3.0 | 0.36 | -3.65 | 0.47 | 120° | 0.51 ± 0.10 | 26.6 ± 1.9 | 0.019 ± 0.004 |
| 4.0 | 0.47 | -0.98 | 0.08 | 45° | 9.4 ± 1.0 | 307 ± 17 | 0.031 ± 0.004 |
| 4.0 | 0.47 | -1.68 | 0.15 | 60° | 1.8 ± 0.3 | 99 ± 7 | 0.018 ± 0.004 |
| 4.0 | 0.45 | -2.49 | 0.22 | 75° | 0.26 ± 0.06 | 10.0 ± 1.0 | 0.027 ± 0.007 |
| 4.0 | 0.44 | -3.36 | 0.33 | 90° | 0.20 ± 0.06 | 7.3 ± 0.7 | 0.027 ± 0.009 |
| 4.0 | 0.45 | -4.23 | 0.47 | 105° | 0.11 ± 0.03 | 4.6 ± 0.5 | 0.025 ± 0.008 |
| 5.0 | 0.58 | -2.45 | 0.21 | 65° | 0.14 ± 0.04 | 3.9 ± 0.4 | 0.037 ± 0.011 |
| 5.0 | 0.55 | -4.29 | 0.40 | 90° | 0.20 ± 0.009 | 1.46 ± 0.10 | 0.014 ± 0.006 |
| 6.0 | 0.61 | -2.45 | 0.16 | 58° | 0.17 ± 0.02 | 3.66 ± 0.25 | 0.048 ± 0.008 |

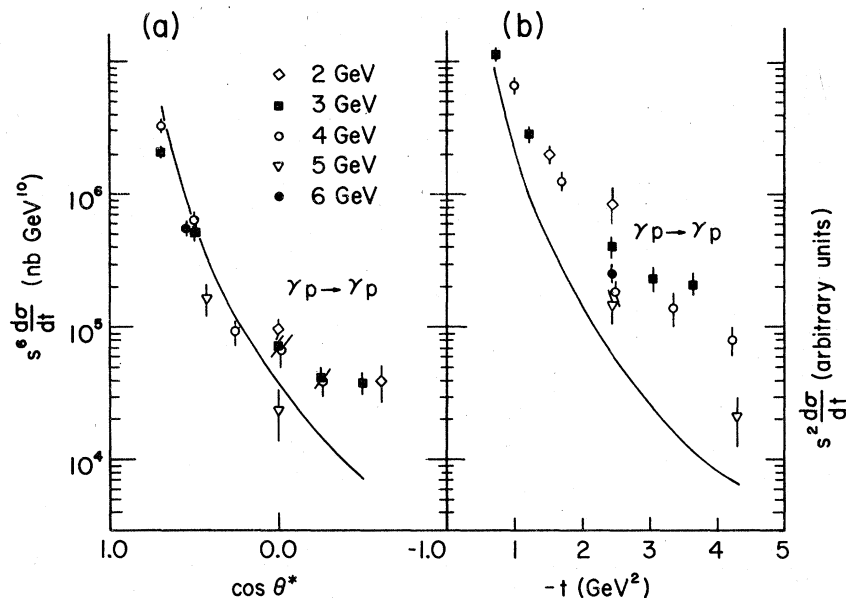


FIG. 5. (a) A test of the dimensional-counting prediction for Compton scattering. The solid line is the prediction of Scott (Ref. 6) at asymptotic s and t . (b) A test for existence of $J=0$ fixed pole in the Compton amplitude (see text). The solid line exhibits t^{-4} dependence.

A. Proton Compton scattering

As shown in Fig. 4(a), the data at large $|t|$ are in sharp contrast to those at small $|t|$. The $|t|$ dependence has become less strong, and there is considerable energy dependence. Some parton models,^{6,7} by considering Compton scattering from individual quarks, predict that at fixed center-of-mass angles, θ^* , far from the forward and backward regions, the proton Compton scattering cross-section energy dependence should vary as $d\sigma/dt \propto s^{-6}$. As shown in Fig. 5(a), the data are in good qualitative agreement with this hypothesis.

Brodsky, Close, and Gunion⁶ (BCG) have predicted that $d\sigma/dt \propto s^{-2}t^{-4}$, and a prediction by Scott⁶ is conceptually similar. Scott continues the Bjorken and Paschos calculation¹⁶ of the inelastic Compton cross section to the exclusive limit. His form includes normalization and when extrapolated to asymptotic s and t coincides with the BCG form. Comparison with the data is shown in Fig. 5(a) and agreement appears good for $\cos\theta^* > 0$. However, at finite s and t , Scott's model does not scale as $s^6 d\sigma/dt$ and falls substantially below our data. It is interesting to note that the Bjorken and Paschos prediction also falls substantially below the inelastic Compton scattering data of Caldwell *et al.*¹⁷ Within the framework of the parton models these discrepancies could be understood as a residual contribution from vec-

tor-dominance diagrams and/or the presence of higher-order amplitudes.¹⁸

Damashek and Gilman³ have found evidence for a fixed pole at $J=0$ in the forward Compton ampli-

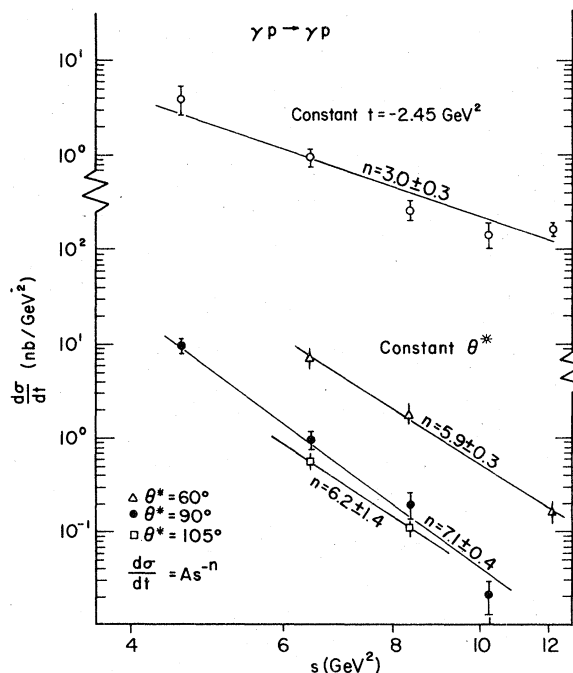


FIG. 6. Compton-scattering cross sections at constant t and at constant θ^* . The straight lines are fits to the data. The fits shown here have no energy cuts.

tude by assuming a Regge form and by use of the photon total cross sections in a dispersion relation. If this real part is due to the Thomson amplitude for photon scattering by partons,⁶ then it should dominate at larger values of t where the diffractive amplitude has died away. In this case the resulting s dependence of the cross section would be s^{-2} . This hypothesis is tested in Fig. 5(b), where the dominance of a fixed pole at $J=0$ would be demonstrated if $s^2 d\sigma/dt$ were independent of s . There is some indication that the higher-energy data far from the backward direction are consistent with this conjecture.

Figure 6 shows energy scans of the data for better comparison with the hypotheses tested by Figs. 5(a) and 5(b). Both sets of data are parametrized by the form $d\sigma/dt = As^{-n}$. For the data at fixed t , $n = 3.0 \pm 0.3$ (the prediction is $n=2$). One might argue that the data point at $s = 4.6 \text{ GeV}^2$ is too low an energy for comparison with models assumed to be valid at asymptotically high energies. If we exclude this point we get $n = 2.6 \pm 0.4$. For fixed $\theta^* > 50^\circ$, the weighted average for n is 6.4 ± 0.3 (the prediction is $n=6$). Excluding the point at $s = 4.6 \text{ GeV}^2$, we get $n = 6.1 \pm 0.3$. These data are in reasonable agreement with the parton-model prediction.

B. π^0 photoproduction

In the central region the t dependence of the π^0 cross section is strikingly different from that of the forward or backward directions. This suggests the existence of a new scattering mechanism, different from t - and u -channel exchanges. The dimensional counting arguments based on a parton structure for hadrons⁷ suggest that at a fixed center-of-mass angle in the central region the cross section $d\sigma/dt$, for charged or neutral-pion photoproduction should be proportional to s^{-7} . Figure 7, where $s^7 d\sigma/dt$ is plotted, shows that the data from the present experiment above 2 GeV are not inconsistent with this dependence. This dependence at 90° is investigated in greater detail in Fig. 8 where some data from other experiments are also included.^{10,11} The agreement seen between our experiment and Anderson *et al.*¹¹ is good at all angles with a χ^2 of 5.7 for 6 degrees of freedom, and both experiments disagree with earlier measurements.¹⁰ Fitting our data to the form $d\sigma/dt = As^{-n}$, we find $n = 9.0 \pm 0.1$. If we adopt the point of view that $s = 4.6 \text{ GeV}^2$ is too low an energy to be compared with predictions intended to be used at asymptotic energies and fit the data at $s = 6.5 \text{ GeV}^2$ and above, we get $n = 8.3 \pm 0.2$. A weighted average for $\theta^* > 50^\circ$ without and with the energy cut gives 8.6 ± 0.1 and 8.0 ± 0.1 , respectively. This is not quantitatively consistent with dimensional counting

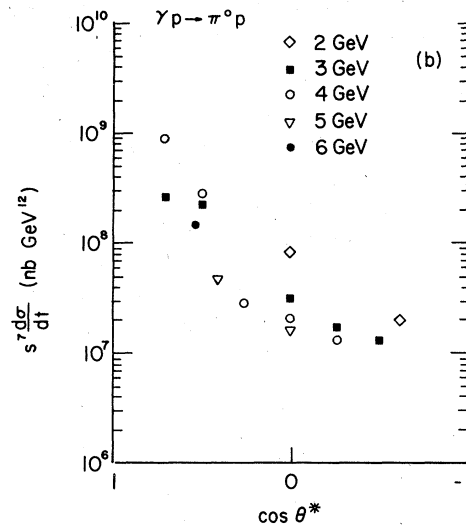


FIG. 7. $s^7 d\sigma/dt$ for π^0 photoproduction versus $\cos \theta^*$.

predictions, but suggests that higher energies may show a more favorable comparison. Anderson *et al.*¹¹ find $n = 7.6 \pm 0.7$ for π^0 photoproduction and $n = 7.3 \pm 0.4$ for π^+ photoproduction for energy ranges similar to ours.

The constituent-interchange type of model^{7,19}

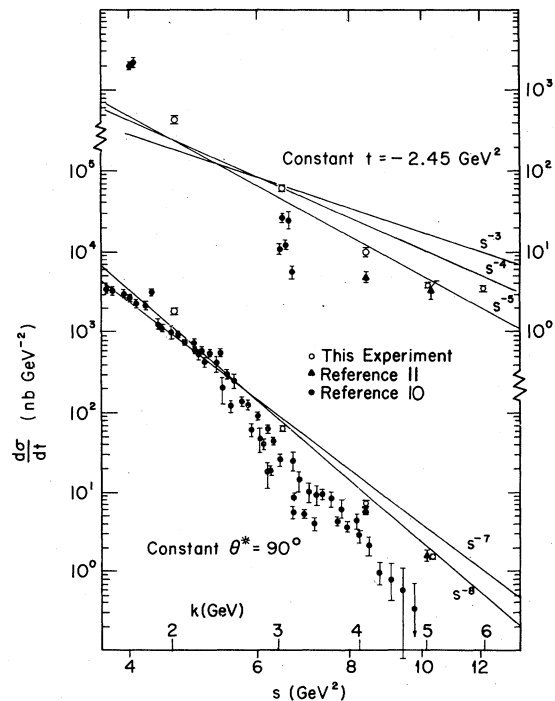


FIG. 8. Log-log plots of $d\sigma/dt$ versus s for π^0 photoproduction. The upper data are at fixed $t = -2.45 \text{ GeV}^2$, while the lower data are at fixed center-of-mass angle, $\theta^* = 90^\circ$.

leads to the prediction that the effective Regge trajectory for pion photoproduction $\alpha(t)$ approaches $-\frac{1}{2}$ at large $|t|$, which means that the cross section will be proportional to s^{-3} at fixed t . Figure 8 also shows the data plotted as a function of s at fixed $t = -2.45 \text{ GeV}^2$. Fitting these data to the same form as above gives $n = 5.0 \pm 0.1$. Eliminating the lowest-energy data point from the fit gives $n = 4.5 \pm 0.2$, although the shape of the data is not well reproduced in either case. The data of Ref. 11 suggest that there is a narrow dip in the cross section near the value of t for which we chose to do our energy scan. If this is so, then $t = -2.45 \text{ GeV}^2$ may not seem a good value for comparison with theory. However, our acceptance in t is broad so that the effects of this dip may well be small.

C. Cross-section ratios

Most systematic errors cancel when we calculate the ratio of the cross sections,

$$R(s, t) = \frac{d\sigma/dt(\gamma p \rightarrow \gamma p)}{d\sigma/dt(\gamma p \rightarrow \pi^0 p)}$$

Taking the ratio of the energy dependence predicted by dimensional counting arguments,⁷ one expects that at fixed θ^* $R(s, t) \propto s^{1.0}$. Figure 9(a) shows $R(s, t)$ at fixed $\theta^* > 50^\circ$. Fitting the data at each angle to the form $R(s, t) = A s^n$ and taking a weighted average gives $n = 2.0 \pm 0.3$. Using the same arguments for pion photoproduction as in the previous section,^{7,19} we then expect to see $R(s, t) \propto s^{1.0}$ at fixed t . In Fig. 9(b), $R(s, t)$ is plotted at fixed $t = -2.45 \text{ GeV}^2$. Fitting the data to the same form as above gives $n = 1.8 \pm 0.4$. Neither of these results is in good agreement with predictions. From the data on the individual processes we conclude that the π^0 prediction is the source of this disagreement.

A test of the vector-dominance model (VDM) in its traditional form has been described in detail elsewhere¹² and is shown in Fig. 4(a). Within the framework of a number of models of hadron structure,^{7,18} the ratio data can be considered as

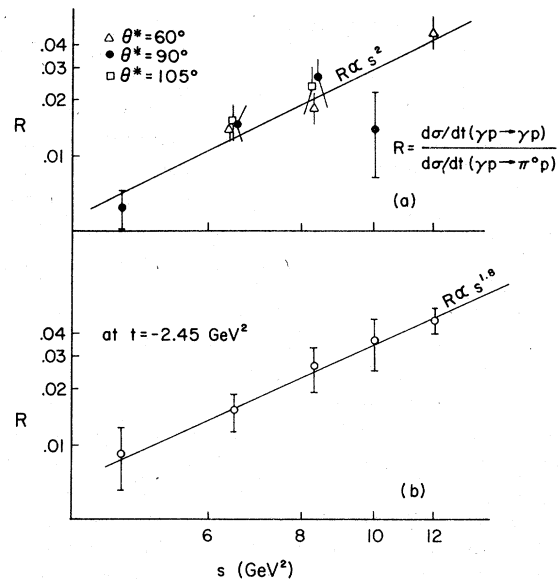


FIG. 9. Compton scattering to π^0 photoproduction cross-section ratios at (a) constant θ^* , and (b) constant t .

an additional test of VDM. These models suggest that the energy dependence of $d\sigma/dt$ at fixed θ^* for vector-meson photoproduction, should be the same as that for neutral-pion photoproduction. The data of Ref. 11 are consistent with this prediction. We can, therefore, consider the data in Fig. 9(a) to show that the ratio of the Compton data to the VDM prediction changes with energy. This is inconsistent with the ideas of the vector-dominance model.

ACKNOWLEDGMENTS

This work was funded through NSF, ERDA, and a University of Massachusetts Faculty Research Grant. It is a pleasure to acknowledge the support and assistance of the Wilson Synchrotron Laboratory staff, and the many useful theoretical discussions with S. Brodsky.

*Now at Dept. of Physics, University of Illinois, Urbana, IL 61801.

†Now at Decision Analysis Group, Stanford Research Institute, Menlo Park, CA 94025.

‡Now at Dept. of Physics, University of Washington, Seattle, WA 98195.

§Now at Computer Sciences Corp., Silver Spring, MD 20910.

||Now at David Rittenhouse Lab., University of Pennsylvania, Philadelphia, PA 19104.

¹M. Deutsch *et al.*, Phys. Rev. D **8**, 3828 (1973), and

references cited therein.

²G. Buschhorn *et al.*, Phys. Lett. **37B**, 207 (1971); A. M. Boyarski *et al.*, Phys. Rev. Lett. **26**, 1600 (1971); **30**, 1098 (E) (1973).

³M. Gell-Mann, M. L. Goldberger, and W. E. Thirring, Phys. Rev. **95**, 1612 (1954); M. Damashek and F. J. Gilman, Phys. Rev. D **1**, 1319 (1970); M. J. Creutz, S. D. Drell, and E. A. Paschos, Phys. Rev. **178**, 2300 (1969).

⁴G. Buschhorn *et al.*, Phys. Lett. **37B**, 211 (1971).

⁵M. Deutsch *et al.*, Phys. Rev. Lett. **29**, 1752 (1972).

- ⁶S. J. Brodsky, F. E. Close, and J. F. Gunion, Phys. Rev. D 5, 1384 (1972); 6, 177 (1972); D. M. Scott, *ibid.* 10, 3117 (1974).
- ⁷S. J. Brodsky and G. R. Farrar, Phys. Rev. Lett. 31, 1153 (1973); V. A. Matveev, R. M. Muradyan, and A. N. Tavkhelidze, Lett. Nuovo Cimento 7, 719 (1973).
- ⁸R. L. Anderson *et al.*, Phys. Rev. D 4, 1937 (1971), and references cited therein.
- ⁹D. Tompkins *et al.*, Phys. Rev. Lett. 23, 725 (1969).
- ¹⁰P. Joos, DESY-HERA Report No. 70-1, 1970 (unpublished). This is a compilation of data. See references therein.
- ¹¹R. L. Anderson *et al.*, Phys. Rev. D 14, 679 (1976).
- ¹²M. A. Shupe *et al.*, Phys. Rev. Lett. 40, 271 (1978).
- ¹³R. A. Early, SLAC Report No. SLAC-TN-66-15, 1966 (unpublished).
- ¹⁴M. A. Shupe, Ph.D. thesis, Tufts University, 1976 (unpublished).
- ¹⁵R. H. Siemann *et al.*, Nucl. Instrum. Methods 129, 427 (1975).
- ¹⁶J. D. Bjorken and E. A. Paschos, Phys. Rev. 185, 1975 (1969).
- ¹⁷D. O. Caldwell *et al.*, Phys. Rev. Lett. 33, 868 (1974).
- ¹⁸R. Blakenbecker and S. J. Brodsky, Phys. Rev. D 10, 2973 (1974).
- ¹⁹J. F. Gunion, in *Particles and Fields—1974*, proceedings of the 1974 Williamsburg meeting of the Division of Particles and Fields of the American Physical Society, edited by Carl E. Carlson (AIP, New York, 1975). Also see Brodsky and Farrar, Ref. 7.